Air turbine Optimisation for OWC Wave Energy Converters: Sensitivity of Realistic Wave Climates

Ander Zarketa-Astigarraga, Maialen Agirre-Aspiazu, Alain Martin-Mayor, Kerman Castro, Aimar Maeso, Manex Martinez-Agirre, Borja de Miguel & Markel Penalba

Abstract—**Among all the Wave Energy Converter (WEC) technologies suggested in the last decades, the Oscillating Water Column (OWC) technology seems to be the most robust and reliable technology. One of the key elements of the OWC technologies is the power take-off (PTO) system that converts the pneumatic energy trapped in the chamber into electrical energy. The most common turbine, mainly due to its relative simplicity both on the conceptual and mechanical aspects, is the Wells monoplane turbine. The preliminary design of these turbines usually relies on analytical models based on the blade element method (BEM), using dimensionless parameters for representing the behavioural charts of the different configurations. In fact, in order to better represent the behaviour of air turbines in realistic conditions with polychromatic waves, it is usual to consider the stochastic version of these dimensionless parameters. However, the air turbines, regardless of their configuration, include a large number of different geometrical parameters, which complicates the optimisation procedure and leads to a decision-making process that relies on an expertise-based intuition. In this sense, an already proposed Genetic Algorithm (GA) based method allows articulating all the relevant parameters. This GA-based optimisation method includes information about the hydrodynamic behaviour of the WEC and the pneumatic conversion within the chamber. Hence, the optimisation is sensitive to the characteristics of the wave climate and, thus, the behaviour of the WEC in that specific wave climate.**

Index Terms—**Wave Energy, Oscillating Water Column, Wells turbine, Genetic Algorithms, Design Optimisation, Wave Climates**

I. Introduction

Concerns about climate change have led to international cooperation, with the Paris Agreement advocating for net zero commitments [1]. Subscriber countries aim to reduce emissions by 45% by 2030 and achieve near-zero emissions by 2050 [2]. Replacing carbon-based energy sources with renewables is a crucial goal. Offshore renewable energy remains largely untapped but has significant potential for decarbonizing the energy system [3]–[5]. Offshore wind is commercialized, while tidal and wave energy are developing. Wave energy, despite its lower maturity, can contribute to the energy transition due to its consistent and compatible energy flow [6].

Among wave converter prototypes, oscillating water column (OWC) devices seem to be one of the most promising technologies [7]–[11], being a robust and reliable solution to extract the untapped energy from ocean waves. The operational principle of OWCs is centered in the internal air chamber, which is submerged in the water, capturing the wave energy through oscillations of the water column inside the chamber. Hence, OWC devices can be either fixed onshore in a breakwater or floating devices deployed offshore. The pneumatic energy stored in the chamber is converted into mechanical energy by means of a bi-directional air turbine, being the Wells turbine [12] the most commonly used in OWCs. Wells turbines are well-known for their simplicity and self-rectification.

Studies have explored turbine modifications, such as biplane configurations and guide vanes, to enhance efficiency [9], [13]. Design parameters, including solidity and hub-to-tip ratio, impact turbine performance [13], [14]. Since then, several studies have analysed these effects by means of experimental and numerical means.

Experimental tests on Wells turbines have provided valuable insights into their behavior. Studies on different turbine configurations have shown that higher values of solidity result in increased swirl downstream of the rotor and decreased overall efficiency. Overall, moderate values of solidity and hub-to-tip ratio are recommended for achieving high efficiencies or controlling the slope of the pressure-flow curve [15]. On the other hand, low values of both parameters are preferred to extend the stall-free operation regime and mitigate acoustic noise caused by stalled blades [15], [16]. Besides the turbine configuration and geometry, different aspects have also been evaluated:

- However, the use of guide vanes, particularly in biplane turbines, helps mitigate this effect [9], [14], [17].
- The use of end plates, which modify the gap between the tip and casing, has been found to increase efficiency by reducing tipward three-dimensional effects [18], [19].

Ander Zarketa-Astigarraga, Alain Martin-Mayor and Manex Martinez-Agirre are with Fluid Mechanics, Mondragon University, Loramendi 4, 20500 Arrasate, Spain. (e-mail: azarketa@mondragon.edu).

Aimar Maeso, Kerman Castro and Borja de Miguel are with IDOM Consulting, Engineering, Architecture S.A.U., Bilbao, Spain.

Maialen Agirre is with Fluid Mechanics, Mondragon University, Loramendi 4, 20500 Arrasate, Spain and IDOM Consulting, Engineering, Architecture S.A.U., Bilbao, Spain.

Markel Penalba is with Fluid Mechanics, Mondragon University, Loramendi 4, 20500 Arrasate, Spain and Ikerbasque, Basque Foundation for Science, Euskadi Plaza 5, Bilbao, Spain. (e-mail: mpenalba@mondragon.edu).

Digital Object Identifier:
https://doi.org/10.36688/ewtec-2023-493

- The spanwise distributions of blade skew, pitch angle, and chordal dimensions also influence turbine behavior [15], [16], [19]–[23].
- Swept blades offer improved efficiency over a wider range of operating conditions, albeit with a reduction in peak efficiency [21]. Furthermore, swept blades can reduce acoustic noise by up to 4 dB compared to unswept baseline turbine blades, while extending the stall-free operating range by 106% [15].
- Pitching the blades improves starting characteristics, lowers operational speed requirements, reduces aerodynamic losses, and enhances overall efficiency compared to baseline configurations [20].

Similarly, numerical investigations of Wells turbines have also been extensively conducted [24]–[30], including studies where numerical and experimental approaches are combined [10], [15], [31]. Earlier computational fluid dynamics (CFD) simulations employed Reynolds-Averaged Navier-Stokes (RANS) with the $k-\varepsilon$ turbulence model to replicate experimental results, showing good agreement in both pre- and post-stall conditions [24]. However, CFD simulations have exhibited limitations in accurately reproducing near-stall conditions [15]. Based on such CFD simulations, improvements of traditional turbine configurations, mostly Wells turbines, have been suggested, such as minor geometric modifications, including radiused edge tips, extended trailing edges, variable blade thicknesses, Gurney flaps, and sharkskin-based riblets [28]–[30]. Similarly, blade pitch variations, demonstrating a slight increase in turbine efficiency aligned with experimental trends [27].

Commonly, the optimisation of the air turbines, regardless of the turbine configuration, is carried out by treating the air turbine as an isolated element operating at steady flows. In fact, advanced optimisation strategies have been applied [10], [27], [32]–[39].Among the available optimisation techniques, genetic algorithms (GA) based on evolutionary programming have gained prominence and are widely utilized for optimising Wells turbine designs [39].

However, the operation of turbines implemented in OWCs is significantly different. On the one hand, the assumption of steady flows is unrealistic, since the common operation in OWCs includes considerably variable conditions in terms of flow and pressure. On the other hand, the hydro-pneumatic performance of the OWC device and, more specifically, the OWC chamber, is tightly connected with the performance of the turbine. Therefore, both aspects should ideally be considered in the optimisation of these turbines. In addition, any optimisation strategy should also consider a realistic representation of the wave climate where the OWC device with the turbine is intended to be deployed.

The variability of the flow can be considered following a stochastic representation of the sea states and, as a consequence, modelling the air turbine as a stochastic process [40]. In fact, it has been shown that this stochastic feature of the wave resource has a critical effect on the energetic outcome of the Wells turbines [9], [17]. Additionally, the validity of the stochastic process for considering the variable performance is also demonstrated.

In contrast, the combination of hydrodynamics and pneumatic effects in OWC WECs, and the aerodynamics of Wells turbines introduces a novel and complex optimisation scenario. As a consequence, [41] suggests a novel holistic optimisation tool for the design of Wells turbines under realistic wave climates. Based on this optimisation tool, the impact of realistic waves climates on the final design of the air turbines is evaluated. Hence, the present paper is structured as follows: Section II briefly explains the methodology of the optimisation tool referring to [41] for further details, Section III describes the case study analysed in this study, Section IV presents and discusses the results of the optimisation, and Section V draws the main conclusions.

II. Methodology

The general procedure of the optimisation tool is illustrated in Fig. 1 including the different sets of inputs and the different stages of the optimisation routine. A comprehensive description of the optimisation process is provided in [41] and a brief explanation of the methodology is given in this section. Overall, the methodology is divided into three main parts: the definition of the input parameters described in Section II-A, the mathematical model for evaluating the performance of the different turbine configurations analysed in the process is presented in Section II-B, and the definition and rationale of the fitness function on which the optimisation is based is in Section II-C.

A. Definition of the input space

The set of input parameters are divided into three different sets:

- Geometrical parameters include the main geometrical aspects that are known to have a significant impact on the aerodynamic performance of the turbine. These parameters are:
  - The number of blades: Z.
  - The radius at the hub: r_{hub}.
  - The hub-to-tip-ratio: ν.
  - Tip clearance percentage: t.
  - Chord distribution along the radius: $c(r)$.
  - The solidity along the radius: $\sigma(r)$.
  - The distribution of the NACA airfoil profile along the radius: $NACA(r)$.
  - The discretisation of the blade.
- WEC and wave climate parameters define the interaction between the hydrodynamic and pneumatic effects in the OWC chamber, and the aerodynamic performance of the turbine, including constraints and control parameters. In this respect, four main parameters have been incorporated:
  - The site-specific weight of each sea state considered in the definition of the realistic wave climate: ω_{SS}

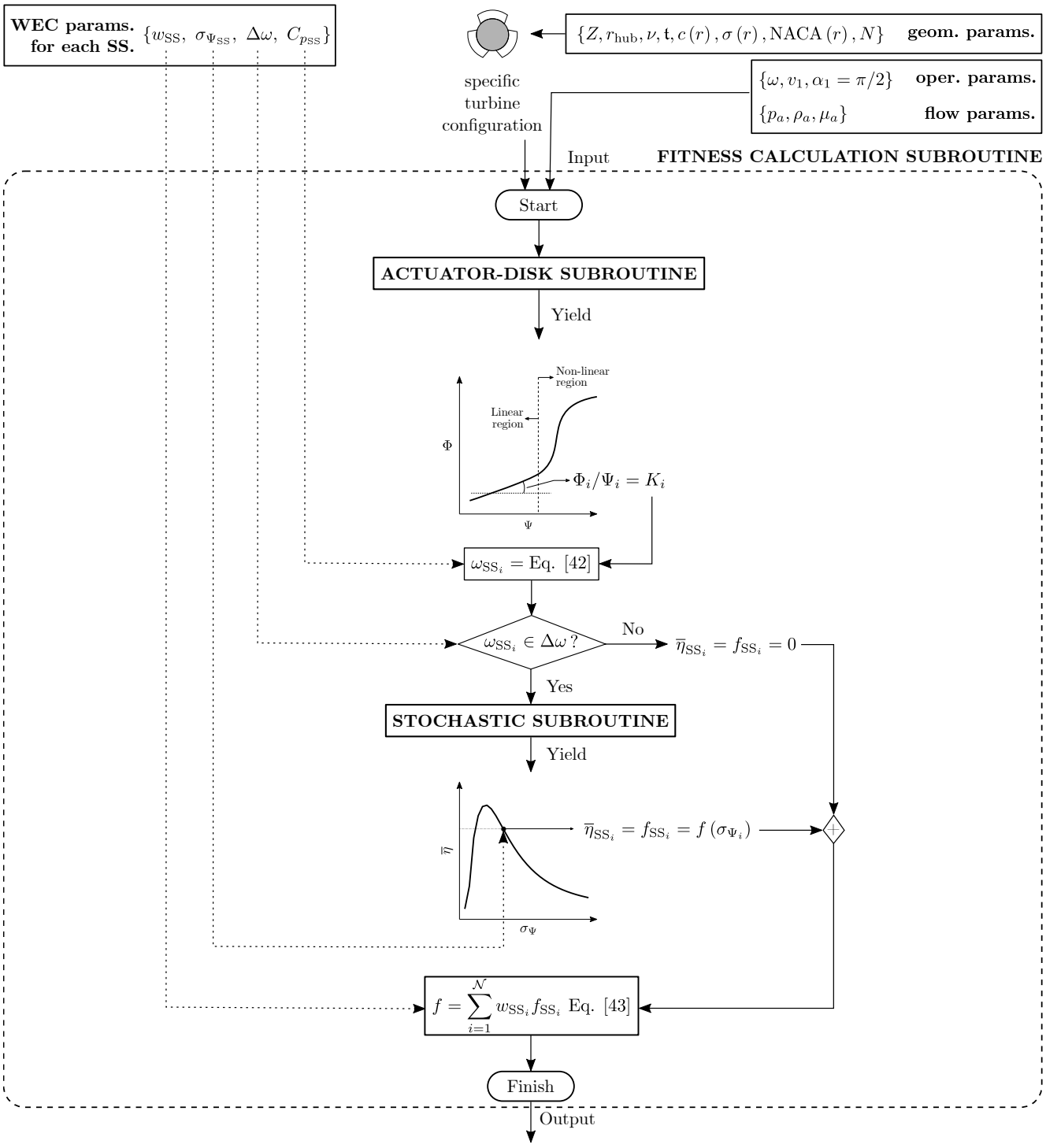

Fig. 1: Flowchart of the optimisation tool [41].

- The standard deviation of the pressure in the OWC chamber: $\sigma_{\Phi_{SS}}$.
- Lower- and upper-constraints of the rotational speed: $\Delta\omega$.
- Damping coefficient for the hydrodynamic control of the OWC WEC at each sea state: C_{pSS}.

B. Performance evaluation

The performance of each air turbine, regardless of its geometrical characteristics and operational conditions, is evaluated by means of an analytical model based on the blade element method (BEM) incorporating the actuator-disk model. Such aerodynamic analytical tools for Wells turbines abound in the literature [10], [42]–[46]. All these analytical models provide the non-dimensional coefficients (given as a function of ω and turbine diameter D_{tip}) that are commonly used for the assessment of the turbine's performance: the flow (Φ), power (Π), pressure-drop (Ψ) and efficiency (η) coefficients.

$$\Pi = \frac{P}{\rho_a \omega^3 D_{\text{tip}}^5}\ , \quad \Psi = \frac{\Delta p}{\rho_a \omega^2 D_{\text{tip}}^2}\ , \quad \eta = \frac{\Pi}{\Psi\Phi}\ , \qquad (1)$$

Further explanation of the analytical BEM/actuator-

disk approach with all the detail for its reproduction and the validation of the model are provided in [41].

However, in addition to the BEM/actuator-disk approach described above, the assessment of a Wells turbine under realistic wave conditions requires the implementation of the stochastic coefficients, as suggested in [40]. The stochastic variability of ocean waves is assumed to follow a Gaussian process and, thus, so does the pressure oscillation in the OWC chamber, whose mean and standard deviation are denoted by p and σ, respectively. Following [17], this leads to the following probability density function (PDF) of p:

$$f\left(p\right)=\frac{1}{\sqrt{2\pi}\sigma}\exp\left(-\frac{p^2}{2\sigma^2}\right)\ . \tag{2}$$

With the stochastic nature of the sea-state (SS) being expressed by the PDF above, the averaged values of the air flow rate (Q), the power output (P), and the pneumatic power available to the turbine ($P_{\text{av.}}=pQ$) are given by:

$$\left\{\overline{Q}\left(\sigma\right),\overline{P}\left(\sigma\right),\overline{P}_{\text{av.}}\left(\sigma\right)\right\}=\frac{1}{\sqrt{2\pi}\sigma}\int_{-\infty}^{\infty}\exp\left(-\frac{p^2}{2\sigma^2}\right)\left\{Q\left(p\right),P\left(p\right),P_{\text{av.}}\left(p\right)\right\}\mathrm{d}p\ , \tag{3}$$

which, in dimensionless variables, adopt the form:

$$\left\{\overline{\Phi}\left(\sigma_\Psi\right),\overline{\Pi}\left(\sigma_\Psi\right),\overline{\Pi}_{\text{av.}}\left(\sigma_\Psi\right)\right\}=\frac{1}{\sqrt{2\pi}\sigma_\Psi}\int_{-\infty}^{\infty}\exp\left(-\frac{\Psi^2}{2\sigma_\Psi^2}\right)\left\{f_\Phi\left(\Psi\right),f_\Pi\left(\Psi\right),\Psi f_\Phi\left(\Psi\right)\right\}\mathrm{d}\Psi\ , \tag{4}$$

showing that the computation of the stochastic curves results from a convolution of the corresponding variables with the Gaussian PDF. Besides, $f_\Phi\left(\Psi\right)$ and $f_\Pi\left(\Psi\right)$ represent the functional relations between $\Phi-\Psi$ and $\Pi-\Psi$, respectively, for a range of input velocities upon which the stochastic analysis is computed. The dimensionless variables shown above are defined as:

$$\overline{\Phi}=\frac{\overline{Q}}{\omega D_{\text{tip}}^3}\ ,\quad \overline{\Pi}=\frac{\overline{P}}{\rho_a\omega^3D_{\text{tip}}^5}\ ,\quad \overline{\Pi}_{\text{av.}}=\frac{\overline{P}_{\text{av.}}}{\rho_a\omega D_{\text{tip}}^5}\ , \tag{5}$$

with $\sigma_\Psi=\sigma/\rho_a\omega^2D_{\text{tip}}^2$ being the dimensionless counterpart of the pressure oscillation p. Similarly, the average efficiency is:

$$\overline{\eta}\left(\sigma_\Psi\right)=\frac{\overline{\Pi}\left(\sigma_\Psi\right)}{\overline{\Pi}_{\text{av.}}\left(\sigma_\Psi\right)}\ . \tag{6}$$

C. Fitness function

The fitness function (f) that provides the performance of a turbine under a realistic wave climate considering all the main sea states is built upon the combination of the outcomes of the stochastic process, and the WEC and wave climate parameters, as illustrated in Fig. 1. To that end, first, the fitness value of an isolated turbine configuration (f_{SS_i}), defined as the aerodynamic stochastic efficiency of the turbine for a single SS, is computed. Then, this isolated fitness value is combined with the occurrence probability of that sea state in a particular site or location (ω_{SS_i}). Hence, the overall fitness value corresponds to a weighted average of the stochastic efficiencies obtained for each sea-state, which results in a sea-state-pondered optimisation:

$$f=\sum_{i=1}^{\mathcal{N}}w_{\text{SS}_i}f_{\text{SS}_i}\ . \tag{7}$$

Finally, the optimisation method utilised in this study, as described in [41], incorporates a parallelised Genetic Algorithm (GA) to enhance the computational efficiency. By parallelising the GA algorithm, the number of evaluations required is significantly reduced, enabling a more efficient sampling of the search space. This optimisation strategy allows for a more streamlined and computationally efficient process, enabling effective exploration of the parameter space and identification of optimal turbine configurations.

III. Case Study

A. Wave conditions

Based on the optimisation tool described in Section II, the optimal geometrical configuration of a monoplane Wells turbine is identified for two different test-sites: i) the Biscay Marine Energy Platform (BIMEP) located in the Bay of Biscay off the Basque coast, and ii) the European Marine Energy Centre (EMEC) located in Orkney islands off the North Scottish coast. Figure 2 (a) shows the locations of the two sites analysed in this study.

The two locations have been selected because of the significant differences in terms of wave conditions, as illustrated in Figs. 2 (b) and (c). The most frequent sea state at BIMEP is about 1.5 m of significant wave height (H_s) and 8.5 s of peak period (T_p), while, at EMEC, the characteristics of the most frequent wave conditions are rather $H_s=0.8$ m and $T_p=6.5$ s. However, the resource at BIMEP seems more consistent, meaning that the most frequent sea state is clearly dominant. In contrast, wave conditions at EMEC seem to have a second relatively dominant peak at about $H_s=2$ m and $T_p=8$ s. Hence, apart from the most frequent conditions, the distribution of the different sea states and their occurrence is significantly different between the two selected test-sites. This is of particular importance for the optimisation, as both the selected sea-states and their occurrence (weights ω_{SS}) vary significantly.

However, the resource at each test-site needs to be reduced to 30 relevant sea states for its consideration in the optimisation tool. In the present study, these 30 most relevant sea states have been selected based on their potential for electricity generation, considering the 30 most energy generating SS. Hence, the green and red markers in Figs. 2 (b) and (c) illustrate the selected 30 SS.

B. Wave energy converter

In addition to the wave climate parameters, the characteristics of the specific OWC WEC for which the turbine is being designed are crucial. In the present

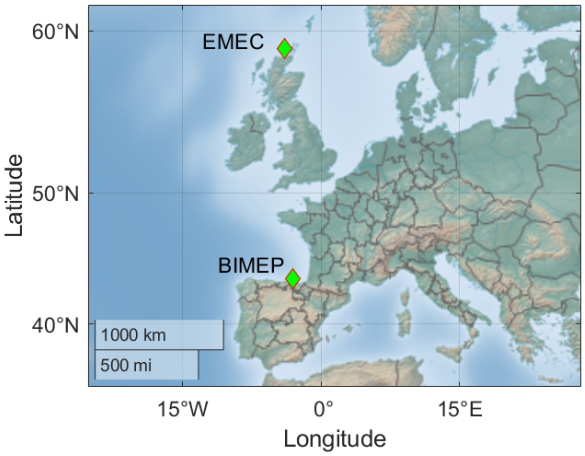

(a) Geographical location.

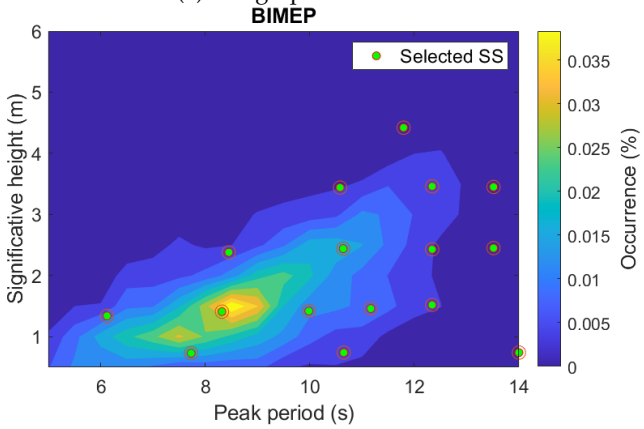

(b) Wave conditions at BIMEP.

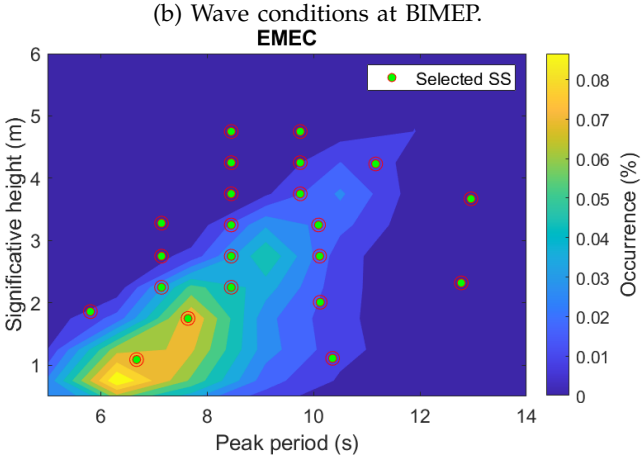

(c) Wave conditions at EMEC.

Fig. 2: Illustration of the main characteristics of the two test-site under evaluation: (a) geographical location, (b) BIMEP wave conditions and (c) EMEC wave conditions.

study, the optimisation study is performed for the floating OWC device MARMOK-A-5 [47], [48] developed by IDOM, which was deployed at the BIMEP test-site [49] for over two and a half years.

The main parameters related to the hydrodynamic and pneumatic performance of the OWC device ($\sigma_{\Phi_{SS}}$ and $C_{p_{SS}}$) are computed from a wave-to-wire simulation model where all the main sub-system and components of the WEC are considered.

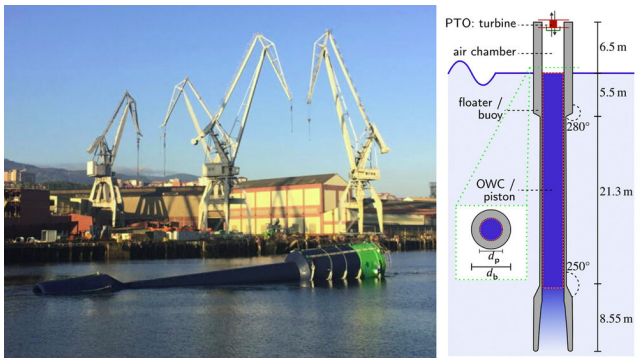

Fig. 3: Illustration of the floating OWC device MARMOK-A-5 developed by IDOM [50].

C. Air turbine

Finally, an initial design of the air turbine has been determined upon which the optimisation is conducted. On the one hand, the turbine configuration is fixed to be a monoplane Wells turbine. On the other hand, no guide vanes and/or potential for pitch variation are considered. In addition, for a preliminary optimisation of the turbine, the input space of the geometrical parameters has been reduced by pre-defining certain parameters, such as the number of blades $Z = 5$, the tip clearance $t = 1\%$ and turbine diameter $D_{tip} = 0.7$ m. Hence, the geometrical parameters to be optimised for each test-site consist on the hub-to-tip ratio ν, solidity along the radial axis $\sigma(r)$, chord distribution along the radial axis $c(r)$ and the distribution of NACA profiles along the radial axis.

IV. Results

Using the optimisation tool described in Section II, the optimal Wells turbine design is identified for the two test-sites and the WEC described in Sections III-A and III-B, respectively.

A. Device performance

Each of the selected SS in both test-sites is simulated via the wave-to-wire model, using the outputs as the inputs for the optimisation procedure. Fig. 4 represents the outputs, both in absolute and relative values, of each SS, illustrating that despite power absorption capabilities of the WEC are maximum for the final SSs, the energy generation along the whole year varies significantly based on the occurrence of each SS. In addition, Fig. 4 represents the control parameter that maximises the final energy generation and the standard deviation of the pressure, both being correlated to the isolated power generation graph. Hence, it is demonstrated that the final power generation and, thus, the turbine optimisation is highly dependent on control parameters and the pneumatic behaviour of the system.

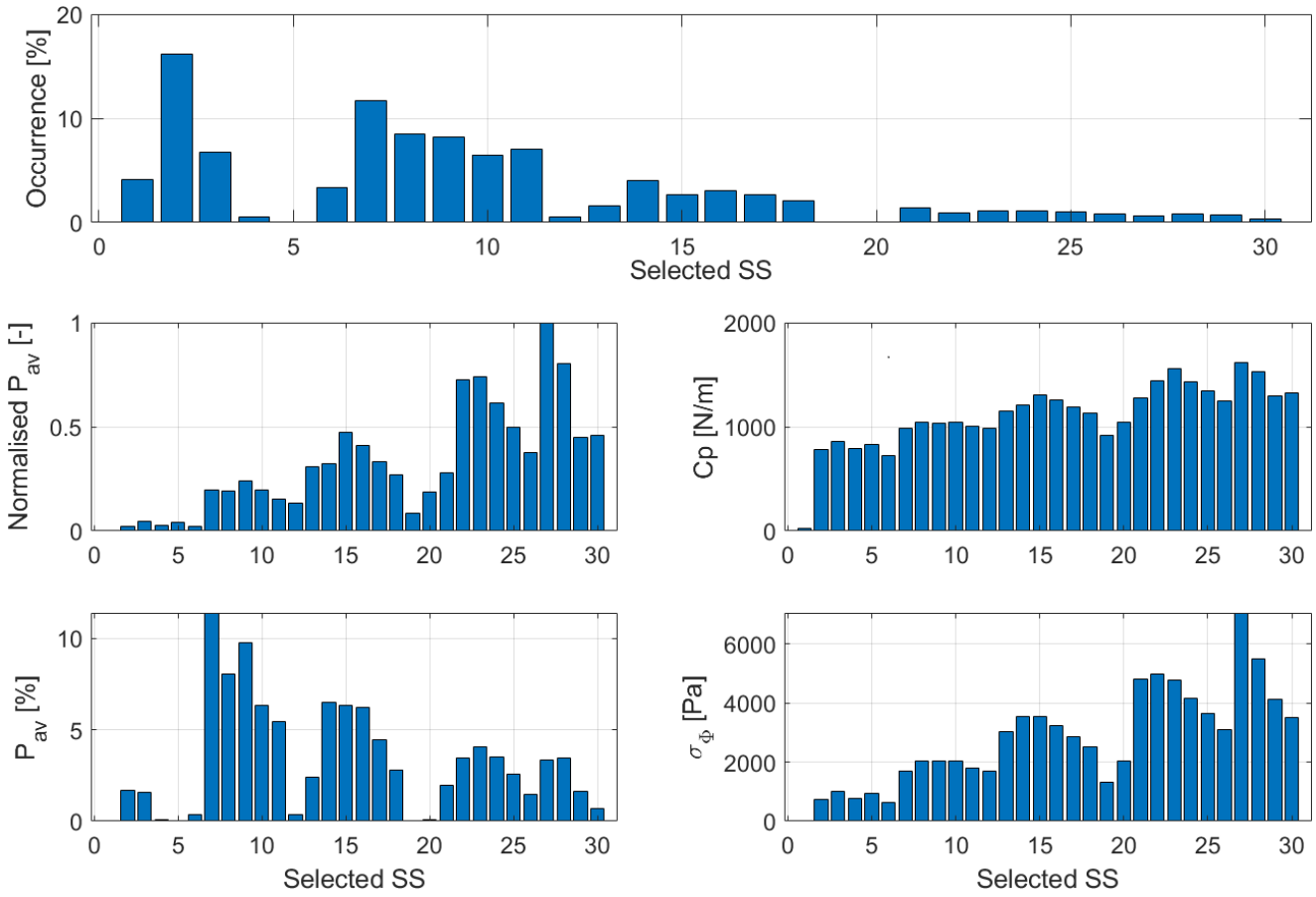

Fig. 4: Performance of the WEC based upon the wave-to-wire simulation at each evaluated SS: (top) occurrence, (middle-left) final power production capabilities of the WEC, (bottom-left) the percentage of the power generation, (middle-right) the control parameter and (bottom-right) standard deviation of the pressure in the OWC chamber.

TABLE I: parameters of the optimal turbine configurations.

Site	ν	Hub			Tip		
		σ	NACA	chord	σ	NACA	chord
BIMEP	0.439	0.667	0013	0.126	0.6	0013	0.263
EMEC	0.4	0.533	0013	0.094	0.567	0014	0.249

B. Turbine optimisation

The results of applying the GA-based approach to the BIMEP and EMEC sites is summarised in Table I, which gathers the geometrical parameters of the optimal turbines. Both the frontal and the cross-sectional views of such turbines have been depicted on Fig. 5. As observed in the frontal view, the EMEC-optimal configuration shows a considerably smaller hub and lower solidity values than the BIMEP-optimal one. The cross-sectional plane shows that the chordal extent of the NACA profiles is appreciably shorter in the case of the EMEC-optimal case, especially at radial stages near the hub. Besides, it is observed that the EMEC-optimal turbine shows a linearly varying NACA distribution, despite such a variation implying a subtle change from a NACA0013 geometry at the hub to a NACA0014 one at the tip. Even so, the higher thickness of the profile is noticeable in the cross-sectional view. As discussed in a recently published paper by the authors [41], the larger blockage of the BIMEP-optimal is indicative that the turbine operates at lower rotational speeds and, accordingly, achieves locating the operational points closer to the maximum stochastic efficiencies.

The translation of the geometrical differences shown in Fig. 5 to efficiency-related terms is shown in Fig. 6, where the left and right columns illustrate the performance of different turbines based upon BIMEP and EMEC conditions, respectively. The plots, as such, synthesise the information concerning the stochastic performance of both optimal turbines when operating in the two considered locations, namely BIMEP and EMEC. Figs. 6a and 6b show the stochastic efficiency curves for the optimal configurations; those curves are reproduced in the two plots, but the operational points shown in each of them correspond to the $\overline{\eta}(\sigma_\Psi)$ values of each optimal turbine obtained for the set of sea-states considered. As observed, the stochastic curve of the BIMEP-optimal configuration lies appreciably higher than the EMEC-optimal one, although both of them show similar maxima. The difference of the curves stem from a milder efficiency drop of the BIMEP-optimal configuration at large values of σ_Ψ. Be-

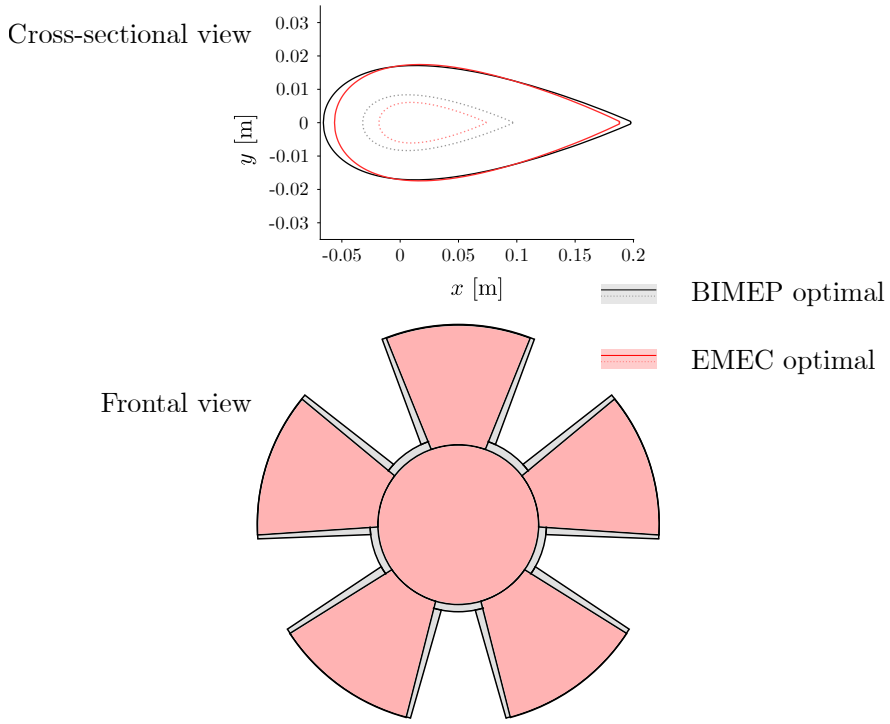

Fig. 5: Front and cross-sectional views of the optimal turbine configurations for the BIMEP and EMEC sites.

sides, and as mentioned before, the larger geometrical blockage of the BIMEP-optimal configuration achieves to cluster its operational points closer to the maximum. Instead, the EMEC-optimal configuration is shown liable to operate at high σ_Ψ values. It is to notice that the main differences between Figs. 6a and 6b is that, in Fig. 6b, the overall set of operational points seems to be sensibly tilted towards the maximum, especially in the case of the BIMEP-optimal configuration. However, the layout of the plots themselves does not allow delving any further into the analysis of the curves.

For such a purpose, Figs. 6c and 6d show, by employing the bar-plots that correspond to the left-side $y-$axis, the individual fitness value adopted by the optimal configurations for each sea-state considered. The line plots, associated to the right-side $y-$axis, represent the cumulative fitness value. It is reminded that the individual fitness is just the product of the stochastic efficiency and the probabilistic weight associated to its correlative sea-state. As such, the data in Figs. 6c and 6d is a broken down surrogate for the operational points shown in 6a and 6b.

The first thing to notice is that the optimal configurations, when operating in the site for which they have been designed, show the best performance. In other words, the BIMEP-optimal configuration achieves the largest cumulative fitness value when operating in the BIMEP site, and the same goes for the EMEC turbine. This behavior is not surprising, and merely shows that the optimization tool works as expected. However, the relative performance differences are remarkable. The EMEC-optimal configuration achieves an overall fitness value of 0.286 compared to the 0.459 value obtained by the BIMEP-optimal one, when both turbines are operating at the BIMEP site. This supposes that the EMEC-optimal turbine shows a relative efficiency drop of 37.69% with respect to the BIMEP-optimal one. Instead, when both turbines are operated at the EMEC site, such fitness values are of 0.269 and 0.228 for the EMEC and BIMEP configurations, respectively. This implies that, even if the EMEC turbine shows the best performance when deployed at its expected site, the BIMEP counterpart merely shows a 15.24% drop in fitness.

These differences in the fitness drops when the optimal turbine configurations are employed in sites other than their nominal ones sets forth two additional considerations. The first has to do with the way in which the configurations achieve the ultimate fitness value or, in other words, the shape of the cumulative lines. On this respect, the BIMEP-optimal turbine seems to prefer a high performance in a relatively low number of sea-states, resulting in cumulative lines that show steep increments combined with milder or even flat regions. Instead, the EMEC-optimal one shows a more constant increasing trend, indicating a relatively lower performance but in a larger number of sea-states than its BIMEP counterpart. Probably, these behavioral trends also explain the geometrical differences shown in Fig. 5. The optimization procedure seems to prefer a BIMEP-optimal turbine with a larger blockage, thus achieving operation points that lie closer to the efficiency maximum and compensate the sacrifice of sea-states in which the turbine would be forced to operate outside its safety bounds, which result in a null fitness value. Instead, the lower-blockage EMEC-optimal configuration overcomes such a limitation by extending its operational range among a larger number of sea-states.

Nevertheless, such a first consideration is not independent from the site conditions at which the turbines operate. Indeed, the distributed nature of the EMEC-

optimal configuration seems to work as expected when at the EMEC site exclusively, given the large loss experienced by the turbine when deployed at BIMEP. But the approach adopted by the BIMEP-optimal configuration seems to be more robust. On this respect, the second relevant point to draw from the analysis is that the optimization procedure may be refined in two ways.

- If the strategies adopted by each of the optimal turbines for maximizing their fitness values remain regardless of the provided, site-related input, one of the first analyses to carry out would imply testing different potential strategies of optimization. In other words, modifying the cost function of the optimization so that the turbines are evaluated, jointly, at the BIMEP and EMEC sites. If a combined optimization shows a better performance than the individual ones, that would mean that the optimization tool allows analysing different maximization strategies that may provide insight into how the geometrical variables of the turbines affect the overall behavior.
- The way in which the site-specific input data is specified may be relevant as well. Fig. 3 shows that the sea-states are determined from power- and occurrence-based criteria. Such criteria may not result in the constitution of a proper clustering of sea-states, and studying the relevance of other parameters may be important on this respect.

V. Conclusion

The present paper has considered GA-based optimizations of Wells turbines subjected to a set of WEC-dependent sea-states at two different sites: BIMEP and EMEC. The analysis of the optimal turbine configurations has revealed the following:

- The geometrical differences of the two configurations show that the relevant aspect determining the behavioral changes among turbines is the relative blockage they induce on the OWC duct. The rest of the geometrical parameters, such as the radial NACA distributions, do not seem to affect the performance of the turbines as sensibly.
- The optimal turbines operate relatively poorer when deployed at sites other than their nominal ones, but the differences in the overall fitness drop are relevant. Whereas the BIMEP-optimal turbine seems more robust to site changes and its fitness value at EMEC lies merely 15% below from that of the EMEC-optimal one, the latter is severely affected and shows a relative efficiency drop over 37% when operating at BIMEP.
- Those differences are traced back to the differing sea-state-wise behaviors adopted by the optimal turbines. Whereas the BIMEP configuration prefers performing with high efficiencies at relatively lower sea-states, the EMEC turbine distributes its lower-efficiency operation points throughout a larger number of sea-states.
- The existence of different strategies paves the way towards launching a campaign with a modified cost function that considers a site-wise joint optimization of the turbines. Likewise, the criteria employed for specifying the site-dependent sea-state input data needs to be further investigated.

Acknowledgements

This publication is part of the research project PID2021-124245OA-I00 funded by MCIN/AEI/10.13039/501100011033 and by ERDF A way of making Europe, the European Union's Horizon 2020 research and innovation EuropeWave programme under the grant No 883751, and the research project funded by the Basque Government's ELKARTEK 2022 program under the grant No. KK-2022/00090. In addition, the authors from the Fluid Mechanics research group at Mondragon University are also supported by the Basque Government's Research Group Program under the grant No. IT1505-22.

References

[1] U. Nations. (2022) The paris agreements. [Online]. Available: https://www.un.org/en/climatechange/paris-agreement
[2] ——. (2022) For a livable climate: Net-zero commitments. [Online]. Available: https://www.un.org/en/climatechange/net-zero-coalition
[3] A. M. Addamo, A. Calvo-Santos, J. Guillén, S. Neehus, A. Peralta-Baptista, G. Petrucco, S. Quatrini, and T. Telsnig, "The EU Blue Economy Report 2022," European Comission, Tech. Rep., 2022.
[4] M. Li, H. Luo, S. Zhou, G. M. Senthil Kumar, X. Guo, T. C. Law, and S. Cao, "State-of-the-art review of the flexibility and feasibility of emerging offshore and coastal ocean energy technologies in East and Southeast Asia," *Renewable and Sustainable Energy Reviews*, vol. 162, no. August 2021, 2022.
[5] H. Hu, W. Xue, P. Jiang, and Y. Li, "Bibliometric analysis for ocean renewable energy: An comprehensive review for hotspots, frontiers, and emerging trends," *Renewable and Sustainable Energy Reviews*, vol. 167, no. June, 2022.
[6] F. Fusco, G. Nolan, and J. Ringwood, "Variability reduction through optimal combination of wind/wave resources: An irish case study," *Energy*, vol. 35, no. 1, pp. 314–325, 2010.
[7] A. F. O. Falcão, "Wave energy utilization: A review of the technologies," *Renewable and Sustainable Energy Reviews*, vol. 14, no. 3, pp. 899–918, 2010.
[8] A. F. Falcão and J. C. Henriques, "Oscillating-water-column wave energy converters and air turbines: A review," *Renewable Energy*, vol. 85, pp. 1391–1424, 2016.
[9] J. S. Alves, L. M. Gato, A. F. Falcão, and J. C. Henriques, "Experimental investigation on performance improvement by mid-plane guide-vanes in a biplane-rotor Wells turbine for wave energy conversion," *Renewable and Sustainable Energy Reviews*, vol. 150, no. October, p. 111497, 2021.
[10] L. Ciappi, I. Simonetti, A. Bianchini, L. Cappietti, and G. Manfrida, "Application of integrated wave-to-wire modelling for the preliminary design of oscillating water column systems for installations in moderate wave climates," *Renewable Energy*, vol. 194, pp. 232–248, 2022.
[11] L. M. Gato, J. C. Henriques, and A. A. Carrelhas, "Sea trial results of the biradial and Wells turbines at Mutriku wave power plant," *Energy Conversion and Management*, vol. 268, no. July, p. 115936, 2022.
[12] A. Wells, "Fluid driven rotary transducer, British Patent Spec. No. 1595700," 1976.
[13] S. Raghunathan, "A methodology for Wells turbine design for wave energy conversion," *Proceedings of the Institution of Mechanical Engineers, Part A: Journal of Power and Energy*, vol. 209, no. 3, pp. 221–232, 1995.
[14] R. Curran and L. M. C. Gato, "The energy conversion performance of several types of wells turbine designs," *Proceedings of the Institution of Mechanical Engineers, Part A: Journal of Power and Energy*, vol. 211, no. 2, pp. 133–145, 1997.
[15] R. Starzmann and T. Carolus, "Effect of blade skew strategies on the operating range and aeroacoustic performance of the wells turbine," *Journal of Turbomachinery*, vol. 136, no. 1, 2013.

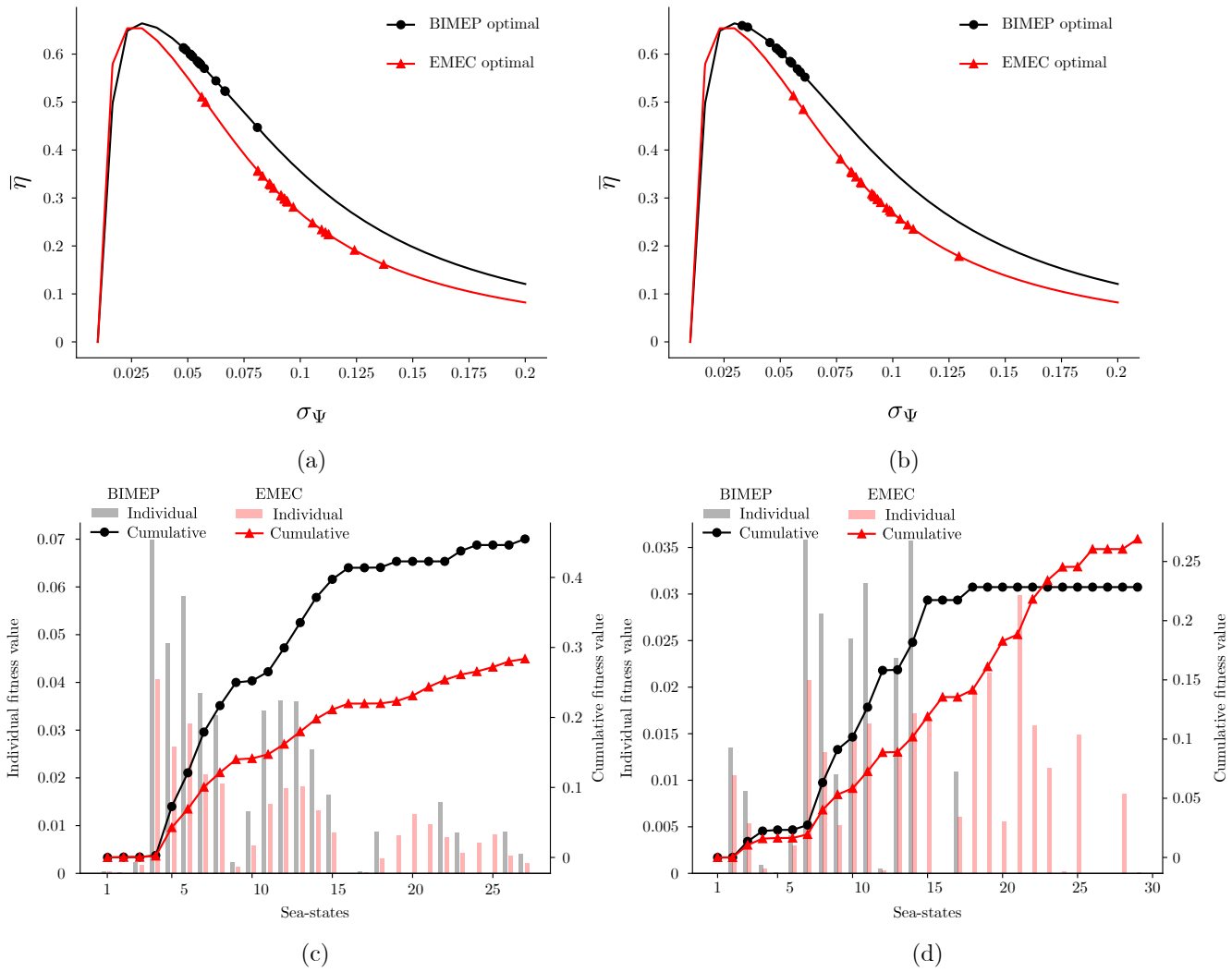

Fig. 6: Efficiency curves and sea-state-wise fitness distributions for the optimal configurations; (a): efficiency curves for the BIMEP site; (b) efficiency curves for the EMEC site; (c) fitness distributions for the BIMEP site; (d) fitness distributions for the EMEC site.

[16] R. Starzmann and T. H. Carolus, "Effect of design parameters on aero-acoustic and aerodynamic performance of Wells turbines," in *Proceedings of the ASME 2011 30th International Conference on Ocean, Offshore and Arctic Engineering*, Rotterdam, The Netherlands, 2011, pp. 1–10.

[17] A. F. Falcão, J. C. Henriques, and L. M. Gato, "Self-rectifying air turbines for wave energy conversion: A comparative analysis," *Renewable and Sustainable Energy Reviews*, vol. 91, no. April, pp. 1231–1241, 2018.

[18] M. Takao, T. Setoguchi, Y. Kinoue, and K. Kaneko, "Wells turbine with end plates for wave energy conversion," *Ocean Engineering*, vol. 34, no. 11, pp. 1790–1795, 2007.

[19] A. S. Shehata, Q. Xiao, K. M. Sqr, and A. Day, "Wells turbine for wave energy conversion: a review," *International Journal of Energy Researc*, pp. 1 –33, 2016.

[20] T. Setoguchi, S. Raghunathan, M. Takao, and K. Kaneko, "Air-turbine with self-pitch-controlled blades for wave energy conversion (estimation of performances in periodically oscillating flow)," in *International Journal of Rotating Machinery*, vol. 3, no. 4, 1997, pp. 233–238.

[21] L. M. C. Gato and M. Webster, "An experimental investigation into the effect of rotor blade sweep on the performance of the variable-pitch wells turbine," *Proceedings of the Institution of Mechanical Engineers, Part A: Journal of Power and Energy*, vol. 215, no. 5, pp. 611–622, 2001.

[22] *Air Turbine Using Self-Pitch-Controlled Blades For Wave Energy Conversion*, ser. International Ocean and Polar Engineering Conference, vol. All Days, 05 2002.

[23] R. Starzmann and T. Carolus, "Model-based selection of full-scale Wells turbines for ocean wave energy conversion and prediction of their aerodynamic and acoustic performances," in *Proceedings of the Institution of Mechanical Engineers, Part A: Journal of Power and Energy*, 2014, pp. 2–16.

[24] T. S. Dhanasekaran and M. Govardhan, "Computational analysis of performance and flow investigation on wells turbine for wave energy conversion," *Renewable Energy*, vol. 30, no. 14, pp. 2129–2147, 2005.

[25] M. Torresi, S. M. Camporeale, P. D. Strippoli, and G. Pascazio, "Accurate numerical simulation of a high solidity Wells turbine," *Renewable Energy*, vol. 33, no. 4, pp. 735–747, 2008.

[26] M. Torresi, S. M. Camporeale, and G. Pascazio, "Detailed CFD analysis of the steady flow in a wells turbine under incipient and deep stall conditions," *Journal of Fluids Engineering, Transactions of the ASME*, vol. 131, no. 7, pp. 0 711 031–07 110 317, 2009.

[27] M. H. Mohamed and S. Shaaban, "Optimization of blade pitch angle of an axial turbine used for wave energy conversion," *Energy*, vol. 56, pp. 229–239, 2013.

[28] P. M. Kumar, P. Halder, A. Husain, and A. Samad, "Performance enhancement of Wells turbine: Combined radiused edge blade tip, static extended trailing edge, and variable thickness modifications," *Ocean Engineering*, vol. 185, no. May, pp. 47–58, 2019.

[29] R. Abbasi and M. J. Ketabdari, "Enhancement of OWC Wells turbine efficiency and performance using riblets covered blades, a numerical study," *Energy Conversion and Management*, vol. 254, no. October 2021, p. 115212, 2022.

[30] A. T. Kotb, M. A. Nawar, Y. A. Attai, and M. H. Mohamed, "Performance assessment of a modified wells turbine using an integrated casing groove and Gurney flap design for wave energy conversion," *Renewable Energy*, vol. 197, no. August, pp. 627–642, 2022.

[31] L. Ciappi, L. Cheli, I. Simonetti, A. Bianchini, G. Manfrida, and L. Cappietti, "Wave-to-wire model of an oscillating-water-column wave energy converter and its application to mediterranean energy hot-spots," *Energies*, vol. 13, no. 21, 2020.

[32] L. M. Gato and J. C. Henriques, "Optimization of symmetrical profiles for the wells turbine rotor blades," *American Society of Mechanical Engineers, Fluids Engineering Division (Publication) FED*, vol. 238, no. July, pp. 623–630, 1996.

[33] M. H. Mohamed, G. Janiga, E. Pap, and D. Thévenin, "Multi-objective optimization of the airfoil shape of Wells turbine used for wave energy conversion," *Energy*, vol. 36, no. 1, pp. 438–446, 2011.

[34] T. Ghisu, G. T. Parks, J. P. Jarrett, and P. J. Clarkson, "Robust design optimization of gas turbine compression systems," *Journal of Propulsion and Power*, vol. 27, no. 2, pp. 282–295, 2011.

[35] S. Shaaban, "Wells turbine blade profile optimization for better wave energy capture," *International Journal of Energy Research*, 2017.

[36] P. Halder, M. H. Mohamed, and A. Samad, "Wave energy conversion: Design and shape optimization," *Ocean Engineering*, vol. 150, no. December 2017, pp. 337–351, 2018.

[37] T. Gratton, T. Ghisu, G. Parks, F. Cambuli, and P. Puddu, "Optimization of blade profiles for the Wells turbine," *Ocean Engineering*, vol. 169, no. August, pp. 202–214, 2018.

[38] A. Mahrooghi and E. Lakzian, "Optimization of Wells turbine performance using a hybrid artificial neural fuzzy inference system (ANFIS) - Genetic algorithm (GA)," *Ocean Engineering*, vol. 226, no. March, 2021.

[39] T. K. Das, E. Kerikous, N. Venkatesan, G. Janiga, D. Thevenin, and A. Samad, "Performance improvement of a Wells turbine through an automated optimization technique," *Energy Conversion and Management: X*, vol. 16, no. August, 2022.

[40] A. F. O. Falcão and R. J. Rodrigues, "Stochastic modelling of OWC wave power plant performance," *Applied Ocean Research*, vol. 24, no. 2, pp. 59–71, 2002.

[41] A. Zarketa-Astigarraga, A. Martin-Mayor, A. Measo, B. de Miguel, M. Martinez-Agirre, and M. Penalba, "A holistic optimization tool for the design of power take-off systems in realistic wave climates: The wells turbine case," *Ocean Engineering*, vol. 285, p. 115332, 2023. [Online]. Available: https://www.sciencedirect.com/science/article/pii/S002980182301716X

[42] S. Raghunathan, C. P. Tan, and N. A. Wells, "Theory and performance of a Wells turbine." *J. Energy*, vol. 6, no. 2 , Mar.-Apr. 1982, pp. 156–160, 1982.

[43] L. M. Gato and A. F. O. Falcão, "On the theory of the wells turbine," *Journal of Engineering for Gas Turbines and Power*, vol. 106, no. 3, pp. 628–633, 1984.

[44] L. M. Gato and A. F. De, "Aerodynamics of the wells turbine," *International Journal of Mechanical Sciences*, vol. 30, no. 6, pp. 383–395, 1988.

[45] ——, "Aerodynamics of the wells turbine: Control by swinging rotor-blades," *International Journal of Mechanical Sciences*, vol. 31, no. 6, pp. 425–434, 1989.

[46] F. Licheri, T. Ghisu, F. Cambuli, and P. Puddu, "Detailed investigation of the local flow-field in a Wells turbine coupled to an OWC simulator," *Renewable Energy*, vol. 197, no. August, pp. 583–593, 2022.

[47] S. Weller, D. N. Parish, D. Trnroos, and L. Johanning, "Open sea OWC motions and mooring loads monitoring at BiMEP," in *Proceedings of the 12th European Wave and Tidal Energy Conference.*, no. August, Cork, Ireland, 2017, pp. 1 –10.

[48] A. A. Carrelhas, L. M. Gato, J. C. Henriques, A. F. Falcão, and J. Varandas, "Test results of a 30 kW self-rectifying biradial air turbine-generator prototype," *Renewable and Sustainable Energy Reviews*, vol. 109, pp. 187–198, 2019.

[49] (2022) Biscay marine energy platform (bimep) - technical characteristics. [Online]. Available: https://www.bimep.com/en/bimep-area/technical-characteristics/

[50] D. Gaebele, M. Magaña, T. Brekken, and O. Sawodny, "State space model of an array of oscillating water column wave energy converters with inter-body hydrodynamic coupling," *Ocean Engineering*, vol. 195, p. 106668, 2020. [Online]. Available: https://www.sciencedirect.com/science/article/pii/S0029801819307851